

Diffusion Partial Differential Equations for Edge Detection

Scott T. Acton
University of Virginia

1	Introduction and Motivation.....	555
1.1	Partial Differential Equations in Image and Video Processing	
1.2	Edges and Anisotropic Diffusion	
2	Background on Diffusion.....	556
2.1	Scale Space and Isotropic Diffusion • 2.2 Anisotropic Diffusion	
3	Anisotropic Diffusion Techniques.....	557
3.1	The Diffusion Coefficient • 3.2 The Diffusion Partial Differential Equation •	
3.3	3.3 Variational Formulation • 3.4 Multiresolution Diffusion • 3.5 Multispectral	
3.4	Anisotropic Diffusion • 3.6. Speckle Reducing Anisotropic Diffusion	
4	Application of Anisotropic Diffusion to Edge Detection	565
4.1	4.1 Edge Detection by Thresholding • 4.2 Edge Detection from Image Features •	
4.2	4.3 Quantitative Evaluation of Edge Detection by Anisotropic Diffusion	
5	Using Vector Diffusion and Parametric Active Contours to Locate Edges.....	568
5.1	5.1 Parametric Active Contours • 5.2 Gradient Vector Flow • 5.3 Motion Gradient	
5.2	Vector Flow	
6	Conclusions.....	570
	References	570

1 Introduction and Motivation

1.1 Partial Differential Equations in Image and Video Processing

The collision of imaging and differential equations makes sense. Without motion or change of scene or changes within the scene, imaging is worthless. First, consider a static environment — we would not need vision in this environment, as the components of the scene are unchanging. In a dynamic environment, however, vision becomes the most valuable sense. Second, consider a constant-valued image with no internal changes or edges. Such an image is devoid of value in the information-theoretic sense.

The need for imaging is based on the presence of change. The mechanism for change in both time and space is described and governed by *differential equations*.

The partial differential equations (PDEs) of interest in this chapter enact *diffusion*. In chemistry or heat transfer, *diffusion* is a process that equilibrates concentration differences without

creating or destroying mass. In image and video processing, we can consider the *mass* to be the pixel intensities or the gradient magnitudes, for example.

These important differential equations are PDEs because they contain partial derivatives with respect to spatial coordinates and to time. These equations, especially in the case of anisotropic diffusion, are nonlinear PDEs because the diffusion coefficient is typically nonlinear.

1.2 Edges and Anisotropic Diffusion

Sudden, sustained changes in image intensity are called *edges*. We know that the human visual system makes extensive uses of edges to perform visual tasks such as object recognition [23]. Humans can recognize complex three-dimensional (3D) objects using only line drawings or image edge information. Similarly, the extraction of edges from digital imagery allows a valuable abstraction of information and a reduction in processing and storage costs. Most definitions of image edges involve some concept of feature scale. Edges are said to exist at

certain scales — edges from detail existing at fine scales and edges from the boundaries of large objects existing at large scales. Furthermore, large-scale edges exist at fine scales, leading to a notion of edge causality.

To locate edges of various scales within an image, it is desirable to have an image operator that computes a scaled version of a particular image or frame in a video sequence. This operator should preserve the position of such edges and facilitate the extraction of the edge map through the *scale space*. The tool of isotropic diffusion, a linear low-pass filtering process, is not able to preserve the position of important edges through the scale space. Anisotropic diffusion, however, meets this criterion and has been used effectively in conjunction with edge detection.

The main benefit of anisotropic diffusion is edge preservation through the image smoothing process. Anisotropic diffusion yields intraregion smoothing, not interregion smoothing, by impeding diffusion at the image edges. The anisotropic diffusion process can be used to retain image features of a specified scale. Furthermore, the localized computation of anisotropic diffusion allows efficient implementation on a locally interconnected computer architecture. Caselles et al. [13] furnish additional motivation for using diffusion in image and video processing. The diffusion methods use localized models where discrete filters become PDEs as the sample spacing goes to zero. The PDE framework allows various properties to be proved or disproved including stability, locality, causality, and the existence and uniqueness of solutions. Through the established tools of numeric analysis, high degrees of accuracy and stability are possible.

In this chapter, we introduce diffusion for image and video processing. We specifically concentrate on the implementation of anisotropic diffusion, providing several alternatives for the diffusion coefficient and the diffusion PDE. Energy-based variational diffusion techniques are also reviewed. Recent advances in anisotropic diffusion processes, including multi-resolution techniques, multispectral techniques, and techniques for ultrasound and radar imagery, are discussed. Finally, the extraction of image edges after anisotropic diffusion is addressed, and vector diffusion processes for attracting active contours to boundaries are examined.

2 Background on Diffusion

2.1 Scale Space and Isotropic Diffusion

To introduce the diffusion-based processing methods and the associated processes of edge detection, let us define some notation. Let I represent an image with real-valued intensity $I(x)$ image at position x in the domain Ω . When defining the PDEs for diffusion, let I_t be the image at time t with intensities $I_t(x)$. Corresponding with image I is the edge map e — the image of “edge pixels” $e(x)$ with Boolean range ($0 = \text{no edge}$,

$1 = \text{edge}$), or real-valued range $e(x) \in [0, 1]$. The set of edge positions in an image is denoted by Ψ .

The concept of *scale space* is at the heart of diffusion-based image and video processing. A scale space is a collection of images that begins with the original, fine-scale image and progresses toward more coarse scale representations. Using a scale space, important image processing tasks such as hierachic searches, image coding, and image segmentation may be efficiently realized. Implicit in the creation of a scale space is the *scale generating filter*. Traditionally, linear filters have been used to scale an image. In fact, the scale space of Witkin [44] can be derived using a Gaussian filter:

$$I_t = G_\sigma * I_0 \quad (1)$$

where G_σ is a Gaussian kernel with standard deviation (scale) of σ , and $I_0 = I$ is the initial image. If

$$\sigma = \sqrt{t}, \quad (2)$$

then the Gaussian filter result may be achieved through an isotropic diffusion process governed by

$$\frac{\partial I_t}{\partial t} = \nabla^2 I_t \quad (3)$$

where $\nabla^2 I_t$ is the Laplacian of I_t [22, 44]. To evolve one pixel of I , we have the following PDE:

$$\frac{\partial I_t(x)}{\partial t} = \nabla^2 I_t(x). \quad (4)$$

The Marr-Hildreth paradigm uses a Gaussian scale space to define multiscale edge detection. Using the Gaussian-convolved (or diffused) images, one may detect edges by applying the Laplacian operator and then finding zero crossings [24]. This popular method of edge detection, called the Laplacian of Gaussian, or LoG, is strongly motivated by the biologic vision system. However, the edges detected from isotropic diffusion (Gaussian scale space) suffer from artifacts such as corner rounding and edge localization error (deviation in detected edge position from the “true” edge position). The localization errors increase with increased scale, precluding straightforward multiscale image/video analysis. As a result, many researchers have pursued anisotropic diffusion as a viable alternative for generating images suitable for edge detection. This chapter focuses on such methods.

2.2 Anisotropic Diffusion

The main idea behind anisotropic diffusion is the introduction of a function that inhibits smoothing at the image edges. This function, called the *diffusion coefficient* $c(x)$, encourages

intraregion smoothing over interregion smoothing. For example, if $c(\mathbf{x})$ is constant at all locations, then smoothing progresses in an isotropic manner. If $c(\mathbf{x})$ is allowed to vary according to the local image gradient, we have anisotropic diffusion. A basic anisotropic diffusion PDE is

$$\frac{\partial I_t(\mathbf{x})}{\partial t} = \operatorname{div}\{c(\mathbf{x})\nabla I_t(\mathbf{x})\} \quad (5)$$

with $\mathbf{I}_0 = \mathbf{I}$ [31].

The discrete formulation proposed in [31] will be used as a general framework for implementation of anisotropic diffusion in this chapter. Here, the image intensities are updated according to

$$[I(\mathbf{x})]_{t+1} = \left[I(\mathbf{x}) + (\Delta T) \sum_{d=1}^{\Gamma} c_d(\mathbf{x}) \nabla I_d(\mathbf{x}) \right]_t, \quad (6)$$

where Γ is the number of directions in which diffusion is computed, $\nabla I_d(\mathbf{x})$ is the directional derivative (simple difference) in direction d at location \mathbf{x} , and time (in iterations) is given by t . ΔT is the time step—for stability, $\Delta T \leq \frac{1}{2}$ in the one-dimensional (1D) case, and $\Delta T \leq \frac{1}{4}$ in the two-dimensional (2D) case using four diffusion directions. For 1D discrete-domain signals, the simple differences $\nabla I_d(\mathbf{x})$ with respect to the “western” and “eastern” neighbors, respectively (neighbors to the left and right), are defined by

$$\nabla I_1(\mathbf{x}) = I(\mathbf{x} - h_1) - I(\mathbf{x}) \quad (7)$$

and

$$\nabla I_2(\mathbf{x}) = I(\mathbf{x} + h_2) - I(\mathbf{x}). \quad (8)$$

The parameters h_1 and h_2 define the sample spacing used to estimate the directional derivatives. For the 2D case, the diffusion directions include the “northern” and “southern” directions (up and down), as well as the “western” and “eastern” directions (left and right). Given the motivation and basic definition of diffusion-based processing, we will now define several implementations of anisotropic diffusion that can be applied for edge extraction.

3 Anisotropic Diffusion Techniques

3.1 The Diffusion Coefficient

The link between edge detection and anisotropic diffusion is found in the edge-preserving nature of anisotropic diffusion. The function that impedes smoothing at the edges is the diffusion coefficient. Therefore, the selection of the diffusion coefficient is the most critical step in performing diffusion-based edge detection. We will review several possible variants of the diffusion coefficient and discuss the associated positive and negative attributes.

To simplify the notation, we will denote the diffusion coefficient at location \mathbf{x} by $c(\mathbf{x})$ in the continuous case. For the discrete-domain case, $c_d(\mathbf{x})$ represents the diffusion coefficient for direction d at location \mathbf{x} . Although the diffusion coefficients here are defined using $c(\mathbf{x})$ for the continuous case, the functions are equivalent in the discrete-domain case of $c_d(\mathbf{x})$. Typically $c(\mathbf{x})$ is a nonincreasing function of $|\nabla I(\mathbf{x})|$, the gradient magnitude at position \mathbf{x} . As such, we often refer to the diffusion coefficient as $c(|\nabla I(\mathbf{x})|)$. For small values of $|\nabla I(\mathbf{x})|$, $c(\mathbf{x})$ tends to unity. As $|\nabla I(\mathbf{x})|$ increases, $c(\mathbf{x})$ decreases to zero. Teboul et al. [40] establish three conditions for edge-preserving diffusion coefficients. These conditions are (a) $\lim_{|\nabla I(\mathbf{x})| \rightarrow 0} c(\mathbf{x}) = M$ where $0 < M < \infty$; (b) $\lim_{|\nabla I(\mathbf{x})| \rightarrow \infty} c(\mathbf{x}) = 0$, and (c) $c(\mathbf{x})$ is a strictly decreasing function of $|\nabla I(\mathbf{x})|$. Property 1 ensures isotropic smoothing in regions of similar intensity, while property 2 preserves edges. The third property is given to avoid numeric instability. While most of the coefficients discussed here obey the first two properties, not all formulations obey the third property.

In [31], Perona and Malik propose

$$c(\mathbf{x}) = \exp\left\{-\left[\frac{\nabla I(\mathbf{x})}{k}\right]^2\right\} \quad (9)$$

and

$$c(\mathbf{x}) = \frac{1}{1 + \left[\frac{\nabla I(\mathbf{x})}{k}\right]^2} \quad (10)$$

as diffusion coefficients. Diffusion operations using (9) and (10) have the ability to sharpen edges (backward diffusion), and are inexpensive to compute. However, these diffusion coefficients are unable to remove heavy-tailed noise and create “staircase” artifacts [42, 49]. See the example of smoothing using (9) on the noisy image in Fig. 1A, producing the result in Fig. 1B. In this case, the anisotropic diffusion operation leaves several outliers in the resultant image. A similar problem is observed in Fig. 2B, using the corrupted image in Fig. 2A as input. You et al. have also shown that (9) and (10) lead to an ill-posed diffusion — a small perturbation in the data may cause a significant change in the result [48].

The inability of anisotropic diffusion to denoise an image has been addressed by Catte et al. [14] and Alvarez et al. [7]. Their regularized diffusion operation uses a modification of the gradient image used to compute the diffusion coefficients. In this case, a Gaussian-convolved version of the image is used in computing diffusion coefficients. Using the same basic form as (9), we have

$$c(\mathbf{x}) = \exp\left\{-\left[\frac{\nabla S(\mathbf{x})}{k}\right]^2\right\} \quad (11)$$

where S is the convolution of I and a Gaussian filter with standard deviation σ :

$$S = I * G_\sigma. \quad (12)$$

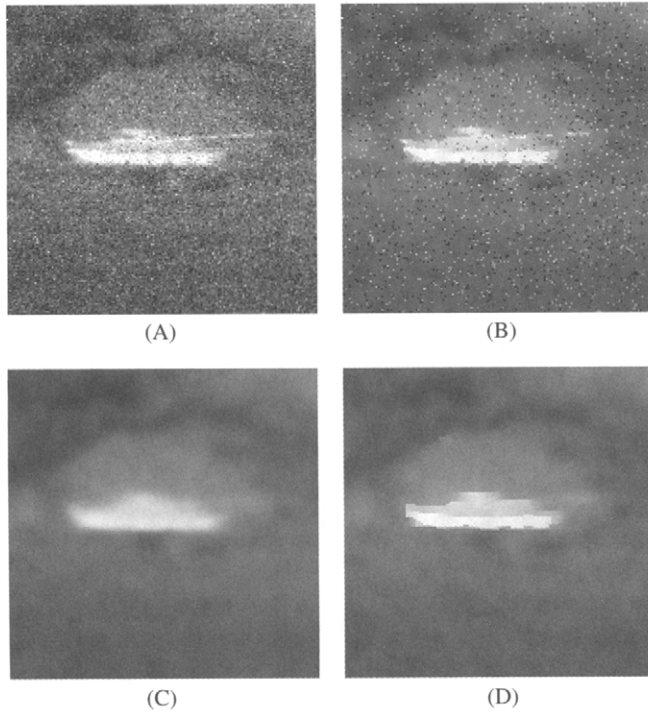


FIGURE 1 Three implementations of anisotropic diffusion applied to an infrared image of a tank: (A) original noisy image; (B) results obtained using anisotropic diffusion with (9); (C) results obtained using modified gradient anisotropic diffusion with (11) and (12); (D) results obtained using morphologic anisotropic diffusion with (11) and (13).

This method can be used to rapidly eliminate noise in the image as shown in Fig. 1C. In this case, the diffusion is well posed and converges to a unique result, under certain conditions [14]. Drawbacks of this diffusion coefficient implementation include the additional computational burden of filtering at each step and the introduction of a linear filter into the edge-preserving anisotropic diffusion approach. The loss of sharpness due to the linear filter is evident in Fig. 2C. Although the noise is eradicated, the edges are softened and blotching artifacts appear in the background of this example result.

Another modified gradient implementation, called *morphologic anisotropic diffusion*, can be formed by substituting

$$\mathbf{S} = (\mathbf{I} \circ \mathbf{B}) \bullet \mathbf{B} \quad (13)$$

into (11), where \mathbf{B} is a structuring element of size $m \times m$, $\mathbf{I} \circ \mathbf{B}$ is the morphologic opening of \mathbf{I} by \mathbf{B} , and $\mathbf{I} \bullet \mathbf{B}$ is the morphologic closing of \mathbf{I} by \mathbf{B} . In [38], the open-close and close-open filters were used in an alternating manner between iterations, thus reducing gray-scale bias of the open-close and close-open filters. As the result in Fig. 1D demonstrates, the morphologic anisotropic diffusion method can be used to eliminate noise and insignificant features while preserving edges. Morphologic anisotropic diffusion has the advantage of selecting feature scale (by specifying the structuring element \mathbf{B}) and selecting the gradient magnitude threshold, whereas

previous anisotropic diffusions, such as with (9) and (10), only allowed selection of the gradient magnitude threshold.

You et al. introduce the following diffusion coefficient in [48]:

$$c(\mathbf{x}) = \begin{cases} 1/T + p(T + \varepsilon)^{p-1}/T, \nabla I(\mathbf{x}) < T \\ 1/|\nabla I(\mathbf{x})| + p(|\nabla I(\mathbf{x})| + \varepsilon)^{p-1}/|\nabla I(\mathbf{x})|, |\nabla I(\mathbf{x})| \geq T \end{cases} \quad (14)$$

where the parameters are constrained by $\varepsilon > 0$ and $0 < p < 1$. T is a threshold on the gradient magnitude, similar to k in (9). This approach has the benefits of avoiding staircase artifacts and removing impulse noise. The main drawback is computational expense. As seen in Fig. 2D, anisotropic diffusion with this diffusion coefficient succeeds in removing noise and retaining important features from Fig. 2A, but requires a significant number of updates.

The diffusion coefficient

$$c(\mathbf{x}) = \frac{1}{|\nabla I(\mathbf{x})|} \quad (15)$$

is used in mean curvature motion formulations of diffusion [35], shock filters [29], and in locally monotonic diffusion [1]. One may notice that this diffusion coefficient is parameter-free.

Designing a diffusion coefficient with robust statistics, Black et al. [8] model anisotropic diffusion as a robust estimation procedure that finds a piecewise smooth representation of an input image. A diffusion coefficient that utilizes the Tukey's biweight norm is given by

$$c(\mathbf{x}) = \frac{1}{2} \left\{ 1 - \left[\frac{|\nabla I(\mathbf{x})|}{\sigma} \right]^2 \right\}^2 \quad (16)$$

for $|\nabla I(\mathbf{x})| \leq \sigma$ and is 0 otherwise. Here, the parameter σ represents scale. Where the standard anisotropic diffusion coefficient as in (9) continues to smooth over edges while iterating, the robust formulation (16) preserves edges of a prescribed scale σ and effectively stops diffusion.

Here, seven important versions of the diffusion coefficient are given that involve tradeoffs between solution quality, solution expense and convergence behavior. Other research in the diffusion area focuses on the diffusion PDE itself. The next section reveals significant modifications to the anisotropic diffusion PDE that affect fidelity to the input image, edge quality, and convergence properties.

3.2 The Diffusion Partial Differential Equation

In addition to the basic anisotropic diffusion PDE given in Section 1.2, other diffusion mechanisms may be employed to adaptively filter an image for edge detection. Nordstrom [28] used an additional term to maintain fidelity to the input image, to avoid the selection of a stopping time, and to avoid

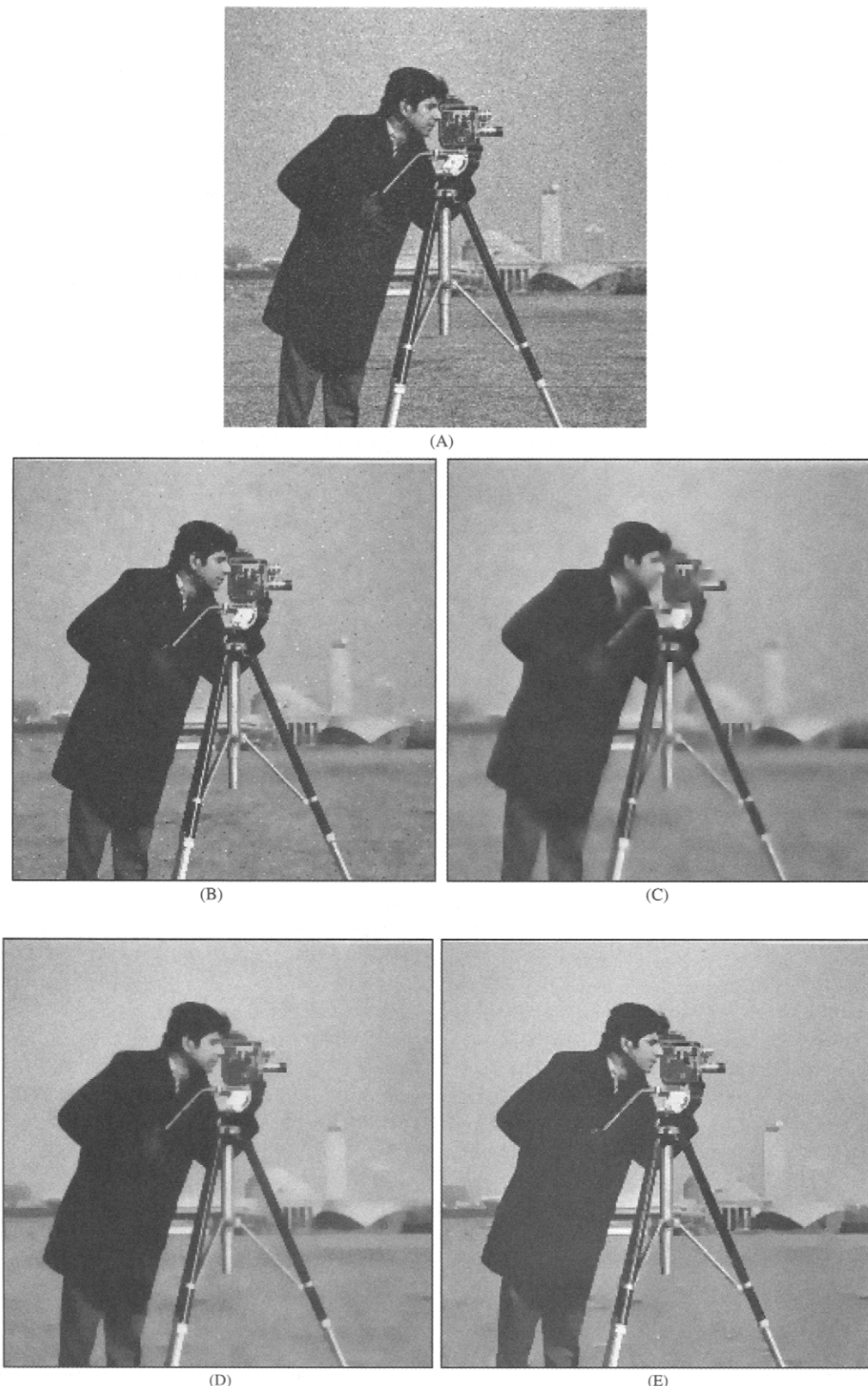


FIGURE 2 (A) Corrupted “cameraman” image (Laplacian noise, SNR=13 dB) used as input for results in Figs. 2(B)–(E); (B) after 8 iterations of anisotropic diffusion with (9), $k = 25$; (C) after 8 iterations of anisotropic diffusion with (11) and (12), $k = 25$; (D) after 75 iterations of anisotropic diffusion with (14), $T = 6$, $e = 1$, $p = 0.5$; (E) after 15 iterations of multigrid anisotropic diffusion with (11) and (12), $k = 6$ [2].

termination of the diffusion at a trivial solution, such as a constant image. This PDE is given by

$$\frac{\partial I_t(\mathbf{x})}{\partial t} - \operatorname{div}\{c(\mathbf{x})\nabla I_t(\mathbf{x})\} = I_0(\mathbf{x}) - I_t(\mathbf{x}). \quad (17)$$

Obviously, the right-hand side $I_0(\mathbf{x}) - I_t(\mathbf{x})$ enforces an additional constraint that penalizes deviation from the input image.

Just as Canny [12] modified the LoG edge detection technique by detecting zero crossings of the Laplacian only in the direction of the gradient, a similar edge-sensitive approach can be taken with anisotropic diffusion. Here, the boundary-preserving diffusion is executed only in the direction

surface in \Re^3 where the image intensity is the third parameter, and each pixel is a graph node. Hence, a color image could be considered a surface in \Re^5 . The curvature motion of the graphs can be used as a model for smoothing and edge detection. For example, let a 3D graph \mathbf{s} be defined by $\mathbf{s}(\mathbf{x}) = \mathbf{s}(x, y) = [x, y, I(x, y)]$ for the 2D image \mathbf{I} with $\mathbf{x} = (x, y)$. To implement mean curvature motion on this graph, the PDE is given by

$$\frac{\partial \mathbf{s}(\mathbf{x})}{\partial t} = h(\mathbf{x})\mathbf{n}(\mathbf{x}) \quad (19)$$

where $h(\mathbf{x})$ is the mean curvature,

$$h(x, y) = \frac{\partial^2 I(x, y)/\partial x^2 \left[1 + (\partial I(x, y)/\partial y)^2 \right] - 2(\partial I(x, y)/\partial x)(\partial I(x, y)/\partial y)(\partial^2 I(x, y)/\partial x\partial y) + \partial^2 I(x, y)/\partial y^2 \left[1 + (\partial I(x, y)/\partial x)^2 \right]}{2 \left[1 + (\partial I(x, y)/\partial y)^2 + (\partial I(x, y)/\partial x)^2 \right]^{3/2}} \quad (20)$$

orthogonal to the gradient direction, whereas the standard anisotropic diffusion schemes *impede* diffusion across the edge. If the rate of change of intensity is set proportional to the second partial derivative in the direction orthogonal to the gradient (called τ), we have

$$\frac{\partial I_t(\mathbf{x})}{\partial t} = \frac{\partial^2 I_t(\mathbf{x})}{\partial \tau^2} = |\nabla I_t(\mathbf{x})| \operatorname{div} \left\{ \frac{\nabla I_t(\mathbf{x})}{|\nabla I_t(\mathbf{x})|} \right\}. \quad (18)$$

This anisotropic diffusion model is called *mean curvature motion*, because it induces a diffusion in which the connected components of the image level sets of the solution image move in proportion to the boundary mean curvature. Several effective edge-preserving diffusion methods have arisen from this framework including [17] and [30]. Alvarez et al. [7] have used the mean curvature method in tandem with the regularized diffusion coefficient of (11) and (12). The result is a processing method that preserves the causality of edges through scale space. For edge-based hierachic searches and multiscale analyses, the edge causality property is extremely important.

The mean curvature method has also been given a graph theoretic interpretation [39, 47]. Yezzi [47] treats the image as a graph in \Re^n — a typical 2D gray-scale image would be a

and $\mathbf{n}(\mathbf{x})$ is the unit normal of the surface:

$$\mathbf{n}(x, y) = \frac{[-\partial I(x, y)/\partial x, -(\partial I(x, y)/\partial x), 1]}{\sqrt{1 + (\partial I(x, y)/\partial y)^2 + (\partial I(x, y)/\partial x)^2}}. \quad (21)$$

For a discrete implementation, the partial derivatives of $I(x, y)$ may be approximated using simple differences. One-sided differences or central differences may be employed. For example, a one-sided difference approximation for $\partial I(x, y)/\partial x$. A central difference approximation for the same partial derivative is given by $\frac{1}{2}[I(x+1, y) - I(x-1, y)]$.

The standard mean curvature PDE (19) has the drawback of edge movement that sacrifices edge sharpness. A remedy to this undesired movement is the use of projected mean curvature vectors. Let \mathbf{z} denote the unit vector in the vertical (intensity) direction on the graph \mathbf{s} . The projected mean curvature diffusion PDE can be formed by

$$\frac{\partial \mathbf{s}(\mathbf{x})}{\partial t} = \{[h(\mathbf{x})\mathbf{n}(\mathbf{x})] \cdot \mathbf{z}\}\mathbf{z}. \quad (22)$$

The PDE for updating image intensity is then

$$\frac{\partial I(\mathbf{x})}{\partial t} = \Delta I(x, y) + k^2 \left[(\partial I(x, y)/\partial x)^2 (\partial^2 I(x, y)/\partial y^2) - 2(\partial I(x, y)/\partial x)(\partial I(x, y)/\partial y)(\partial^2 I(x, y)/\partial x\partial y) + (\partial I(x, y)/\partial y)^2 (\partial^2 I(x, y)/\partial x^2) \right] \frac{\{1 + k^2 [\nabla I(x, y)]^2\}^2}{\{1 + k^2 [\nabla I(x, y)]^2\}^2} \quad (23)$$

where k scales the intensity variable. When k is zero, we have isotropic diffusion, and when k becomes larger, we have a damped geometric heat equation that preserves edges but diffuses more slowly. The projected mean curvature PDE gives edge preservation through scale space.

Another anisotropic diffusion technique leads to locally monotonic signals [1]. Unlike previous diffusion techniques that diverge or converge to trivial signals, locally monotonic (LOMO) diffusion converges rapidly to well-defined LOMO signals of the desired degree. (A signal is locally monotonic of degree d (LOMO- d) if each interval of length d is nonincreasing or nondecreasing.) The property of local monotonicity allows both slow and rapid signal transitions (ramp and step edges) while excluding outliers due to noise. The degree of local monotonicity defines the signal scale. In contrast to other diffusion methods, LOMO diffusion does not require an additional regularization step to process a noisy signal and uses no thresholds or ad hoc parameters.

On a 1D signal, the basic LOMO diffusion operation is defined by (6) with $\Gamma = 2$ and using the diffusion coefficient (15), yielding

$$[I(x)]_{t+1} \leftarrow \left(I(x) + (1/2) \{ \operatorname{sgn}[\nabla I_1(x)] + \operatorname{sgn}[\nabla I_2(x)] \} \right)_t, \quad (24)$$

where a time step of $\Delta T = 1/2$ is used. Equation (24) is modified for the case where the simple difference $\nabla I_1(x)$ or $\nabla I_2(x)$ is zero. Let $\nabla I_1(x) \leftarrow -\nabla I_2(x)$ in the case of $\nabla I_1(x) = 0$; $\nabla I_2(x) \leftarrow -\nabla I_1(x)$ when $\nabla I_2(x) = 0$. The fixed point of (24) is defined as $\operatorname{ld}(\mathbf{I}, h_1, h_2)$, where h_1 and h_2 are the sample spacings used to compute the simple differences $\nabla I_1(x)$ and $\nabla I_2(x)$, respectively (see (7) and (8)). Let $\operatorname{ld}_d(\mathbf{I})$ denote the LOMO diffusion sequence that gives a LOMO- d signal from the input \mathbf{I} . For odd values of $d = 2m + 1$,

$$\begin{aligned} \operatorname{ld}_d(\mathbf{I}) = & \operatorname{ld}(\dots \operatorname{ld}(\operatorname{ld}(\operatorname{ld}(\mathbf{I}, m, m), \\ & m - 1, m), m - 1, m - 1) \dots, 1, 1). \end{aligned} \quad (25)$$

In (25), the process commences with $\operatorname{ld}(\mathbf{I}, m, m)$ and continues with spacings of decreasing widths until $\operatorname{ld}(\mathbf{I}, 1, 1)$ is implemented. For even values of $d = 2m$, the sequence of operations is similar:

$$\begin{aligned} \operatorname{ld}_d(\mathbf{I}) = & \operatorname{ld}(\dots \operatorname{ld}(\operatorname{ld}(\operatorname{ld}(\mathbf{I}, m - 1, m), \\ & m - 1, m - 1), m - 2, m - 1) \dots, 1, 1). \end{aligned} \quad (26)$$

To extend this method to two dimensions, the same procedure may be followed using (6) with $\Gamma = 4$ [1]. Another possibility is diffusing orthogonal to the gradient direction at each point in the image, using the 1D LOMO diffusion. Examples of 2D LOMO diffusion and the associated edge detection results are given in Section 3.

3.3 Variational Formulation

The diffusion PDEs discussed thus far may be considered numeric methods that attempt to minimize a cost or energy functional. Energy-based approaches to diffusion have been effective for edge detection and image segmentation. Morel and Solimini [26] give an excellent overview of the variational methods. Isotropic diffusion via the heat diffusion equation leads to a minimization of the following energy:

$$E(\mathbf{I}) = \int_{\Omega} |\nabla I(\mathbf{x})|^2 d\mathbf{x}. \quad (27)$$

Given an initial image \mathbf{I}_0 , the intermediate diffusion solutions may be considered a descent on

$$E(\mathbf{I}) = \lambda^2 \int_{\Omega} |\nabla I(\mathbf{x})|^2 d\mathbf{x} + \int_{\Omega} [I(\mathbf{x}) - I_0(\mathbf{x})]^2 d\mathbf{x} \quad (28)$$

where the regularization parameter λ denotes scale [26].

Likewise, anisotropic diffusion has a variational formulation. The energy associated with the Perona and Malik diffusion is

$$E(\mathbf{I}) = \lambda^2 \int_{\Omega} C [|\nabla I(\mathbf{x})|^2] d\mathbf{x} + \int_{\Omega} [I(\mathbf{x}) - I_0(\mathbf{x})]^2 d\mathbf{x} \quad (29)$$

where C is the integral of $c'(\mathbf{x})$ with respect to the independent variable $|\nabla I(\mathbf{x})|^2$. Here, $c'(\mathbf{x})$, as a function of $|\nabla I(\mathbf{x})|^2$, is equivalent to the diffusion coefficient $c(\mathbf{x})$ as a function of $|\nabla I(\mathbf{x})|$, so $c'(|\nabla I(\mathbf{x})|^2) = c(|\nabla I(\mathbf{x})|)$. The Nordstrom [28] diffusion PDE (17) yields steepest descent on this energy functional.

Teboul et al. [40] have introduced a variational method that preserves edges and is useful for edge detection. In their approach, image enhancement and edge preservation are treated as two separate processes. The energy functional is given by

$$\begin{aligned} E(\mathbf{I}, \mathbf{e}) = & \lambda^2 \int_{\Omega} \left[e(\mathbf{x})^2 |\nabla I(\mathbf{x})|^2 + k(e(\mathbf{x}) - 1)^2 \right] d\mathbf{x} \\ & + \frac{\alpha^2}{k} \int_{\Omega} \varphi(|\nabla e(\mathbf{x})|) d\mathbf{x} + \int_{\Omega} [I(\mathbf{x}) - I_0(\mathbf{x})]^2 d\mathbf{x} \end{aligned} \quad (30)$$

where the real-valued variable $e(\mathbf{x})$ is the edge strength at position \mathbf{x} , and $e(\mathbf{x}) \in [0, 1]$. In (30), the diffusion coefficient is defined by $c(|\nabla I(\mathbf{x})|) = \varphi'(|\nabla I(\mathbf{x})|)/2(|\nabla I(\mathbf{x})|)$. An additional regularization parameter α is needed, and k is essentially an edge threshold parameter.

The energy functional in (30) leads to a system of two coupled PDEs:

$$I_0(\mathbf{x}) - I_t(\mathbf{x}) - \lambda^2 \operatorname{div}\{e(\mathbf{x})[\nabla I_t(\mathbf{x})]\nabla I_t(\mathbf{x})\} = 0, \quad (31)$$

and

$$e(\mathbf{x}) \left[\frac{|\nabla I(\mathbf{x})|^2}{k} + 1 \right] - 1 + \frac{\alpha^2}{k^2} \operatorname{div}[c(|\nabla e(\mathbf{x})|) \nabla e(\mathbf{x})] = 0. \quad (32)$$

The coupled PDEs have the advantage of edge preservation within the adaptive smoothing process. An edge map can be directly extracted from the final state of e .

This edge-preserving variational method is related to the segmentation approach of Mumford and Shah [27]. The energy functional to be minimized is

$$E(\mathbf{I}) = \lambda^2 \int_{\Omega \setminus \Psi} |\nabla I(\mathbf{x})|^2 d\mathbf{x} + \int_{\Omega \setminus \Psi} [I(\mathbf{x}) - I_0(\mathbf{x})]^2 d\mathbf{x} + \mu \lambda^2 \int_{\Psi} d\Psi, \quad (33)$$

where $\int_{\Psi} d\Psi$ is the integrated length of the edges (Hausdorff measure), $\Omega \setminus \Psi$ is the set of image locations that exclude the edge positions, and μ is additional weight parameter. The additional edge-length term reflects the goal of computing a minimal-length edge map for a given scale λ . The Mumford-Shah functional has spurred several variational image segmentation schemes, including PDE-based solutions [26].

In edge detection, thin, contiguous edges are typically desired. With diffusion-based edge detectors, the edges may be “thick” or “broken” when a gradient magnitude threshold is applied after diffusion. The variational formulation allows the addition of additional constraints that promote edge thinning and connectivity. Black et al. [8] used two additional terms, a hysteresis term for improved connectivity and a nonmaximum suppression term for thinning. A similar approach was taken in [5]. The additional terms allow the effective extraction of spatially coherent outliers. This idea is also found in the design of line processes for regularization [18].

3.4 Multiresolution Diffusion

One drawback of diffusion-based edge detection is the computational expense. Typically, a large number (anywhere from 20 to 200) of iterative steps are needed to provide a high-quality edge map. One solution to this dilemma is the use of multiresolution schemes. Two such approaches have been investigated for edge detection: the anisotropic diffusion pyramid and multigrid anisotropic diffusion.

In the case of isotropic diffusion, the Gaussian pyramid has been used for edge detection and image segmentation

[10, 11]. The basic idea is that the scale-generating operator (a Gaussian filter, for example) can be used as an antialiasing filter before sampling. Then, a set of image representations of increasing scale and decreasing resolution (in terms of the number of pixels) can be generated. This image pyramid can be used for hierarchic searches and coarse-to-fine edge detection.

The anisotropic diffusion pyramids [3, 4] are born from the same fundamental motivation as their isotropic, linear counterparts. However, with a nonlinear scale-generating operator, the pre-sampling operation is constrained morphologically, not by the traditional sampling theorem. In the nonlinear case, the scale-generating operator should remove image features not supported in the subsampled domain. Therefore, morphologic methods [25, 37] for creating image pyramids have also been used in conjunction with the morphologic sampling theorem [20].

The anisotropic diffusion pyramids are, in a way, ad hoc multigrid schemes. A multigrid scheme can be useful for diffusion-based edge detectors in two ways. First, like the anisotropic diffusion pyramids, the number of diffusion updates may be decreased. Second, the multigrid approach can be used to eliminate low frequency error. The anisotropic diffusion PDEs are stiff — they rapidly reduce high frequency error (noise, small details), but slowly reduce background variations and often create artifacts such as blotches (false regions) or staircases (false step edges). See Fig. 3 for an example of a staircasing artifact.

To implement a multigrid anisotropic diffusion operation [2], define \mathbf{J} as an estimate of the image \mathbf{I} . A system of equations is defined by $A(\mathbf{I}) = 0$ where

$$[A(\mathbf{I})](\mathbf{x}) = (\Delta T) \sum_{d=1}^D c_d(\mathbf{x}) \nabla I_d(\mathbf{x}), \quad (34)$$

which is relaxed by the discrete anisotropic diffusion PDE (6). For this system of equations, the (unknown) algebraic error is $\mathbf{E} = \mathbf{I} - \mathbf{J}$, and the residual is $\mathbf{R} = -A(\mathbf{J})$ for image estimate \mathbf{J} . The residual equation $A(\mathbf{E}) = \mathbf{R}$ can be relaxed (diffused) in the same manner as (34) using (6) to form an estimate of the error.

The first step is performing v diffusion steps on the original input image (level $L = 0$). Then, the residual equation at the coarser grid $L + 1$ is

$$A(\mathbf{E}_{L+1}) = -A[(\mathbf{J}_L)_{\downarrow S}] \quad (35)$$

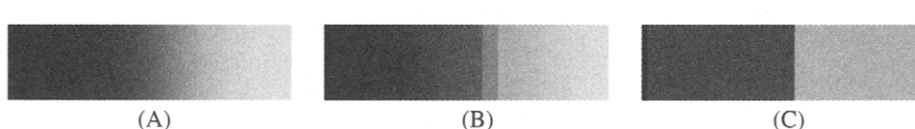


FIGURE 3 (A) Sigmoidal ramp edge; (B) after anisotropic diffusion with (9) ($k = 10$); (C) after multigrid anisotropic diffusion with (9) ($k = 10$) [2].

where $\downarrow S$ represents down-sampling by a factor of S . Now, the residual equation (35) can be relaxed using the discrete diffusion PDE (6) with an initial error estimate of $E_{L+1} = 0$. The new error estimate E_{L+1} after relaxation can then be transferred to the finer grid to correct the initial image estimate J in a simple two-grid scheme. Or, the process of transferring the residual to successively coarser grids can be continued until a grid is reached in which a closed form solution is possible. Then, the error estimates are propagated back to the original grid.

Additional steps may be taken to account for the nonlinearity of the anisotropic diffusion PDE, such as implementing a full approximation scheme (FAS) multigrid system, or by using a global linearization step in combination with a Newton method to solve for the error iteratively [9, 19].

The results of applying multigrid anisotropic diffusion are shown in Fig. 2E. In just 15 updates, the multigrid anisotropic diffusion method was able to remove the noise from Fig. 2B while preserving the significant objects and avoiding the introduction of blotching artifacts.

3.5 Multispectral Anisotropic Diffusion

Color edge detection and boundary detection for multispectral imagery are important tasks in general image/video processing, remote sensing, and biomedical image processing. Applying anisotropic diffusion to each channel or spectral band separately is one possible way of processing multichannel or multispectral image data. However, this single-band approach forfeits the richness of the multispectral data and provides individual edge maps that do not possess corresponding edges.

Two solutions have emerged for diffusing multispectral imagery. The first, called *vector distance dissimilarity*, uses a function of the gradients from each band to compute an overall diffusion coefficient. For example, to compute the diffusion coefficient in the “western” direction on an RGB color image, the following function could be applied:

$$\nabla I_1(\mathbf{x}) = \sqrt{[R(x - h_1, y) - R(x, y)]^2 + [G(x - h_1, y) - G(x, y)]^2 + [B(x - h_1, y) - B(x, y)]^2} \quad (36)$$

where $R(\mathbf{x})$ is the red band intensity at \mathbf{x} , $G(\mathbf{x})$ is the green band, and $B(\mathbf{x})$ is the blue band. Using the vector distance dissimilarity method, the standard diffusion coefficients such as (9) can be used. This technique was used in [43] for shape-based processing and in [6] for processing remotely sensed imagery. An example of multispectral anisotropic diffusion is shown in Fig. 4. Using the noisy multispectral image in Fig. 4A as input, the vector distance dissimilarity method produces the smoothed result shown in Fig. 4B, which has an associated

image of gradient magnitude shown in Fig. 4C. As can be witnessed in Fig. 4C, an edge detector based on vector distance dissimilarity is sensitive to noise and does not identify the important image boundaries.

The second method uses mean curvature motion and a multispectral gradient formula to achieve anisotropic, edge-preserving diffusion. The idea behind mean curvature motion, as discussed above, is to diffuse in the direction opposite to the gradient such that the image level set objects move with a rate in proportion to their mean curvature. With a gray-scale image, the gradient is always perpendicular to the level set objects of the image. In the multispectral case, this quality does not hold. A well-motivated diffusion is defined by Sapiro and Ringach [36], using DiZzenzo’s multispectral gradient formula [16]. In Fig. 4D, results for multispectral anisotropic diffusion are shown for the mean curvature approach of [36] used in combination with the modified gradient approach of [14]. The edge map in Fig. 4E shows improved resilience to impulse noise over the vector distance dissimilarity approach.

3.6 Speckle Reducing Anisotropic Diffusion

The anisotropic diffusion PDE introduced in (5) assumes that the image is corrupted by additive noise. Speckle-reducing anisotropic diffusion (SRAD) is a PDE technique for image enhancement in which signal-dependent multiplicative noise is present, as with radar and ultrasonic imaging. So, where traditional anisotropic diffusion can be viewed as the edge-sensitive version of classic linear filters (e.g., the Gaussian filter), SRAD can be viewed as the edge sensitive version of classic speckle reducing filters that emerged from the radar community (e.g., the Lee filter). SRAD smoothes the imagery and enhances edges by inhibiting diffusion across edges and allowing isotropic diffusion within homogeneous regions. For images containing signal-dependent, spatially correlated multiplicative noise, SRAD excels over the adaptive filtering techniques designed with additive noise models in mind.

The SRAD technique uses an adaptive speckle filter that uses a local statistic for the coefficient of variation, defined as

the ratio of standard deviation to mean, to measure the strength of edges in speckle imagery. A discrete form of this operator in 2D is [50]:

$$q(\mathbf{x}) = \sqrt{\frac{(1/2)|\nabla I(\mathbf{x})|^2 - (1/16)(\nabla^2 I(\mathbf{x}))^2}{[I(\mathbf{x}) + (1/4)\nabla^2 I(\mathbf{x})]^2}}. \quad (37)$$

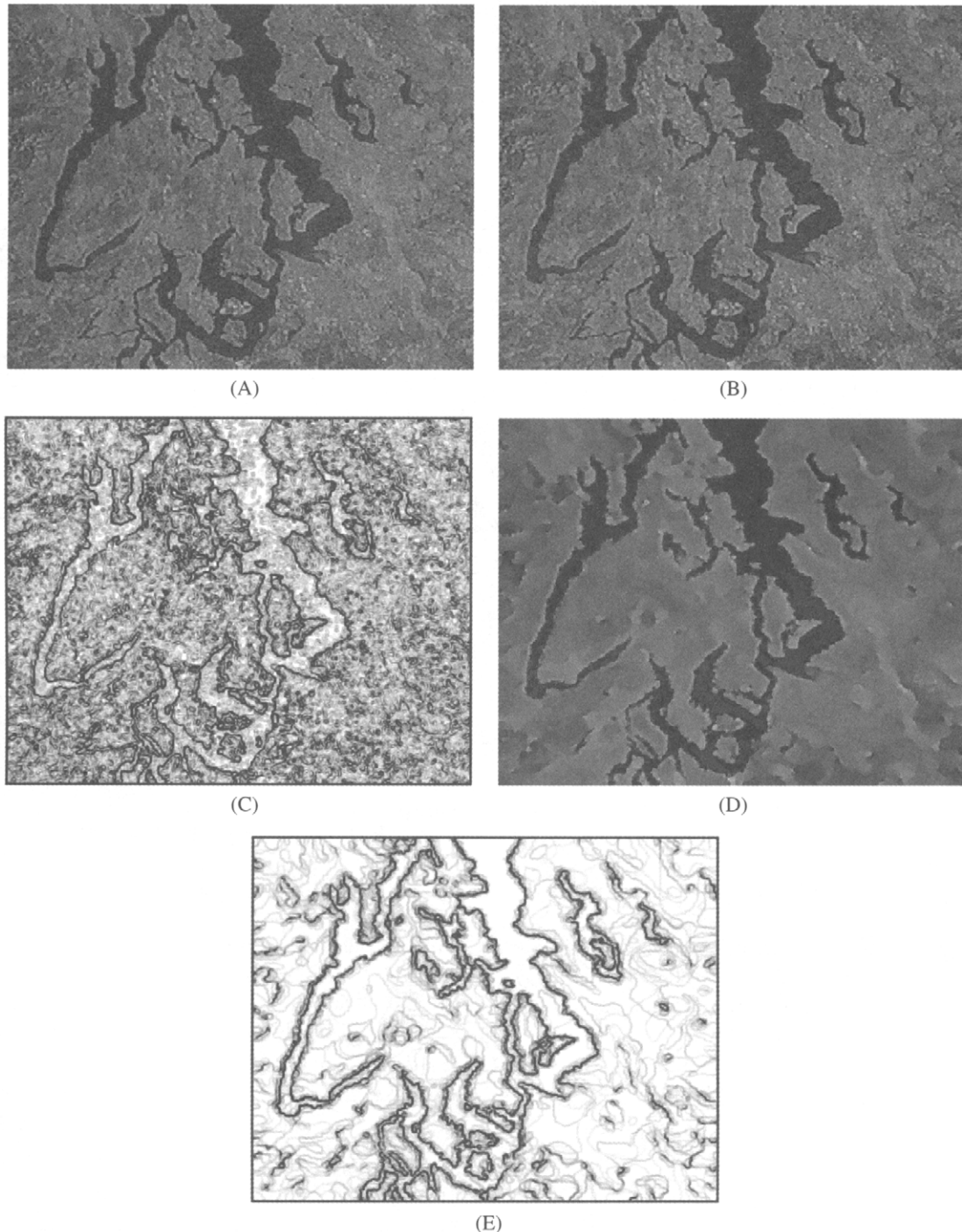


FIGURE 4 (A) SPOT multispectral image of the Seattle area, with additive Gaussian-distributed noise, $\sigma = 10$. (B) Vector distance dissimilarity diffusion result, using diffusion coefficient in (9). (C) Edges (gradient magnitude) from result in (B). (D) Mean curvature motion (18) result using diffusion coefficient from (11) and (12). (E) Edges (gradient magnitude) from result in (D). (See color insert.)

where $\nabla^2 I(\mathbf{x})$ is the Laplacian of image at position \mathbf{x} , and $\nabla I(\mathbf{x})$ is the gradient of image at position \mathbf{x} .

The operator $q(\mathbf{x})$ is called the *instantaneous coefficient of variation* (ICOV). The ICOV uses the absolute value of the difference of a normalized gradient magnitude and a

normalized Laplacian operator to measure the strength of edges in speckled imagery. The normalizing function $I(\mathbf{x}) + (1/4)\nabla^2 I(\mathbf{x})$ gives a smoothed version of the image at position \mathbf{x} . This term compensates for the edge measurement localization error. The instantaneous coefficient of variation

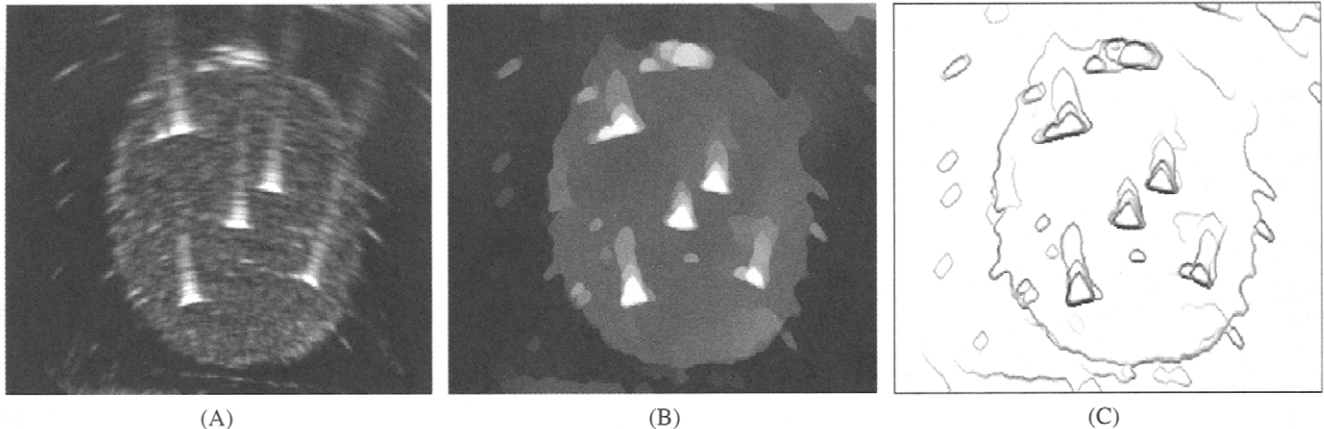


FIGURE 5 (A) An ultrasound image of a prostate phantom with implanted radioactive seeds; (B) corresponding SRAD-diffused image; (C) corresponding ICOV edge strength image [51].

allows for balanced and well-localized edge strength measurements in bright regions as well as in dark regions. It has been shown that the ICOV operator optimizes the edge detection in speckle imagery in terms of low false edge detection probability and high edge localization accuracy [51]. Figure 5 shows an example of an ultrasound image (Fig. 5A) that has been processed by SRAD (Fig. 5B) and where edges are displayed using the ICOV values (Fig. 5C).

Given an intensity image \mathbf{I} having no zero-valued intensities over the image domain, the output image is evolved according to the following PDE:

$$\frac{\partial I_t(\mathbf{x})}{\partial t} = \operatorname{div}[c(q(\mathbf{x})) \nabla I_t(\mathbf{x})] \quad (38)$$

where ∇ is the gradient operator, div is the divergence operator, and $| |$ denotes the magnitude. The diffusion coefficient $c(q(\mathbf{x}))$ is given by

$$c(q(\mathbf{x})) = \left\{ 1 + \frac{[q^2(\mathbf{x}) - \tilde{q}^2(\mathbf{x})]}{\tilde{q}^2(\mathbf{x})(1 + \tilde{q}^2(\mathbf{x}))} \right\}^{-1} \quad (39)$$

where $q(\mathbf{x})$ is the instantaneous coefficient of variation as determined by (37), and $\tilde{q}(\mathbf{x})$ is the current speckle noise level. Example input and output images from an ultrasound image of the human heart are shown in Fig. 6.

The diffusion coefficient $c(q(\mathbf{x}))$ is proportional to the likelihood that a point \mathbf{x} is in a homogeneous speckle region at the update time. From (39), it is seen that the diffusion coefficient exhibits nearly zero values at edges with high contrast (i.e., $q(\mathbf{x}) \gg \tilde{q}(\mathbf{x})$); while in homogeneous speckle regions, the coefficient approaches unity. Hence, it is the diffusion coefficient that allows isotropic diffusion in homogeneous speckle regions and prohibits diffusion across the edges.

The implementation issues connected with anisotropic diffusion include specification of the diffusion coefficient

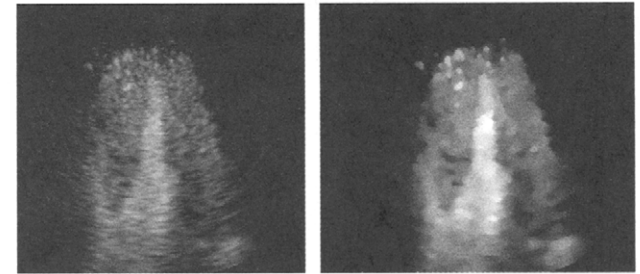


FIGURE 6 (Left) Speckled ultrasound image of left ventricle in a human heart prior to SRAD, (Right) Same image after SRAD enhancement.

and diffusion PDE, as discussed above. The anisotropic diffusion method can be expedited through multiresolution implementations. Furthermore, anisotropic diffusion can be extended to multispectral imagery and to ultrasound/radar imagery. In the following section, we discuss the specific application of anisotropic diffusion to edge detection.

4 Application of Anisotropic Diffusion to Edge Detection

4.1 Edge Detection by Thresholding

Once anisotropic diffusion has been applied to an image \mathbf{I} , a procedure needs to be defined to extract the image edges \mathbf{e} . The most typical procedure is to simply define a gradient magnitude threshold, T , that defines the location of an edge. For example, $e(\mathbf{x}) = 1$ if $|\nabla I(\mathbf{x})| > T$ and $e(\mathbf{x}) = 0$ otherwise. Of course, the question becomes one of selecting a proper value for T . With typical diffusion coefficients such as (9) and (10), $T = k$ is often asserted. Another approach is to use the diffusion coefficient itself as the measure of edge strength: $e(\mathbf{x}) = 1$ if $c(x) < T$ and $e(\mathbf{x}) = 0$ otherwise.

In [8], edges are detected by finding gradient magnitudes that exceed the robust scale ($T = \sigma_e$) of the image, as defined

in [34]: $\sigma_e = 1.4826 \text{med}\{|\nabla I(x) - \text{med}(|\nabla I(x)|)|\}$ where the *med* operator is the median performed over the entire image domain Ω . The constant used (1.4826) is derived from the mean absolute deviation of the normal distribution with unit variance [8].

4.2 Edge Detection from Image Features

Aside from thresholding the gradient magnitude of a diffusion result, a feature detection approach may be used. As with Marr's classic LoG detector, the inflection points of a diffused image may be located by finding the zero crossing in a Laplacian-convolved result. However, if the anisotropic diffusion operation produces piecewise constant images as in [8] and [48], the gradient magnitude is sufficient to define thin, contiguous edges.

With locally monotonic diffusion, other features that appear in the diffused image may be used for edge detection. An advantage of locally monotonic diffusion is that no threshold is required for edge detection. Locally monotonic diffusion segments each row and column of the image into ramp segments and constant segments. Within this framework, we can define *concave-down*, *concave-up*, and *ramp center* edge detection processes. Consider an image row or column. With a concave-down edge detection, the ascending (increasing intensity) segments mark the beginning of an

object and the descending (decreasing intensity) segments terminate the object. With a concave-up edge detection, negative-going objects (in intensity) are detected. The ramp center edge detection sets the boundary points at the centers of the ramp edges, as the name implies. When no bias toward bright or dark objects is present, a ramp center edge detection can be utilized.

Figure 7 provides two examples of feature-based edge detection using locally monotonic diffusion. The images in Fig. 7B and Fig. 7E are the results of applying 2D locally monotonic diffusion to Fig. 7A and Fig. 7D, respectively. The concave-up edge detection given in Fig. 7C reveals the boundaries of the blood cells. In Fig. 7F, a ramp center edge detection is used to find the boundaries between the aluminum grains of Fig. 7D.

4.3 Quantitative Evaluation of Edge Detection by Anisotropic Diffusion

When choosing a suitable anisotropic diffusion process for edge detection, one may evaluate the results qualitatively or use an objective measure. Three such quantitative assessment tools include the percentage of edges correctly identified as edges, the percentage of false edges, and Pratt's edge quality metric. Given ground truth edge information, usually with synthetic data, one may measure the correlation between the

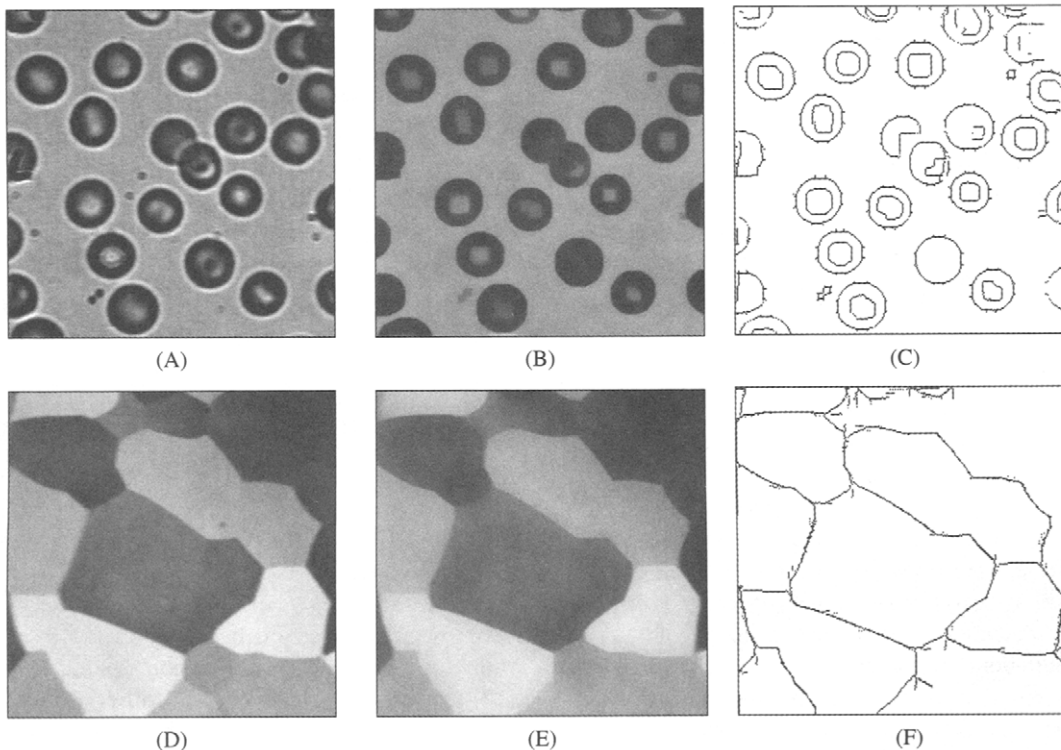


FIGURE 7 (A) Original "Blood Cells" image. (B) 2D LOMO-3 diffusion result. (C) Boundaries from concave-up edge detection of image in (B). (D) Original "Aluminum Grains" image. (E) 2D LOMO-3 diffusion result. (F) Boundaries from ramp center edge detection of image in (E).

ideal edge map and the computed edge map. This correlation leads to a classification of “correct” edges (where the computed edge map and ideal version match) and “false” edges. Another method uses Pratt’s edge quality measurement [32]:

$$F = \frac{\sum_{i=1}^{I_A} \frac{1}{1+\alpha(d(i)^2)}}{\max\{I_A, I_I\}} \quad (40)$$

where I_A is the number of edge pixels detected in the diffused image result, I_I is the number of edge pixels existing in the original, noise free imagery, $d(i)$ is the Euclidean distance

between an edge location in the original image and the nearest detected edge, and α is a scaling constant (with suggested value of 1/9 [32]). A “perfect” edge detection result has value $F=1$ in (40).

An example is given here where a synthetic image is corrupted by 40% salt-and-pepper noise (Fig. 8). Three versions of anisotropic diffusion are implemented on the noisy imagery using the diffusion coefficients from (9), from (11), and (12) and from (11) and (13). The threshold of the edge detector was defined to be equal to the gradient threshold of the diffusion coefficient, $T=k$. The results of the numeric

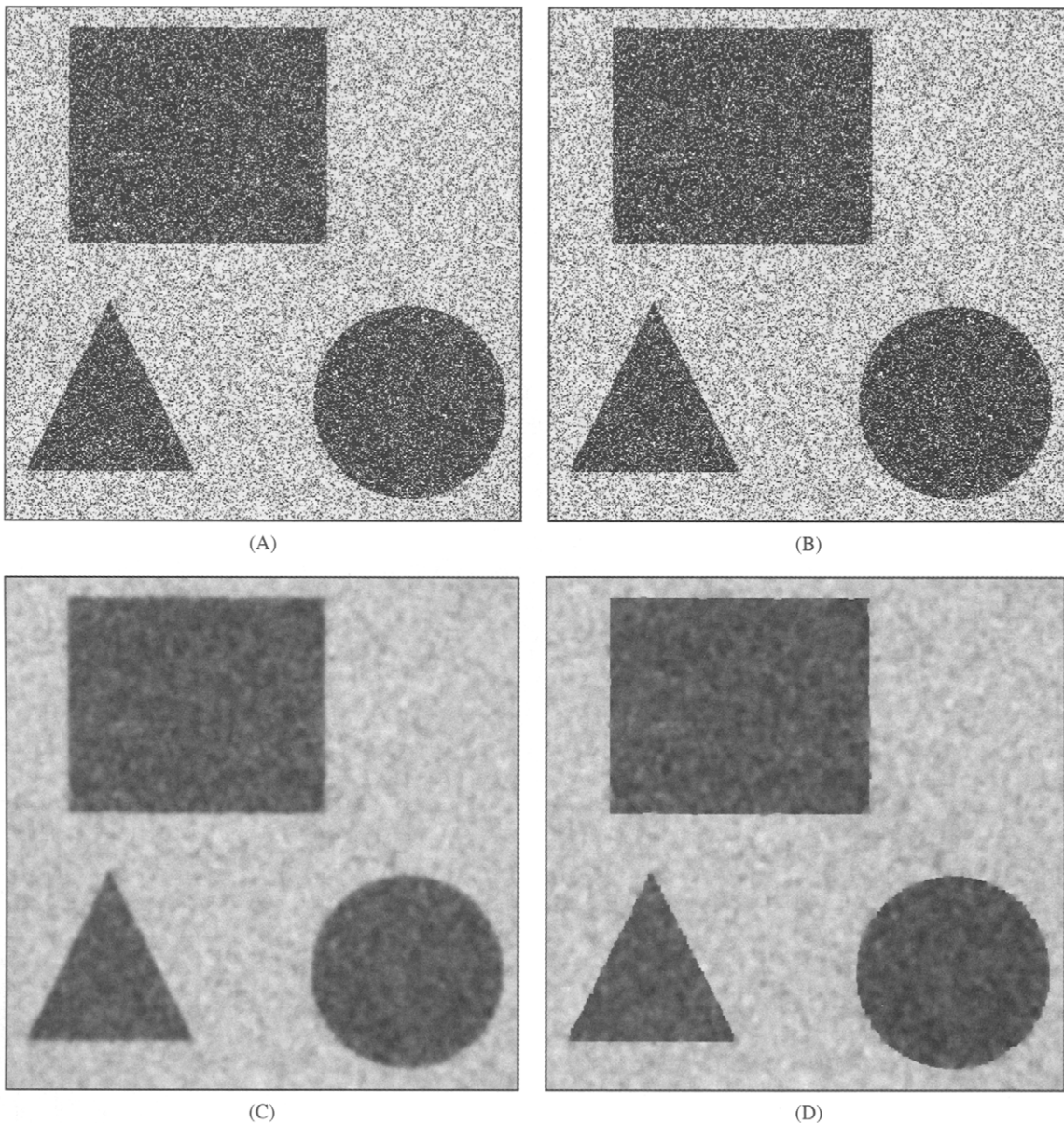


FIGURE 8 Three implementations of anisotropic diffusion applied to synthetic imagery: (A) original image corrupted with 40% salt-and-pepper noise; (B) results obtained using original anisotropic diffusion with (9); (C) results obtained using modified gradient anisotropic diffusion with (11) and (12); (D) results obtained using morphologic anisotropic diffusion with (11) and (13) [38].

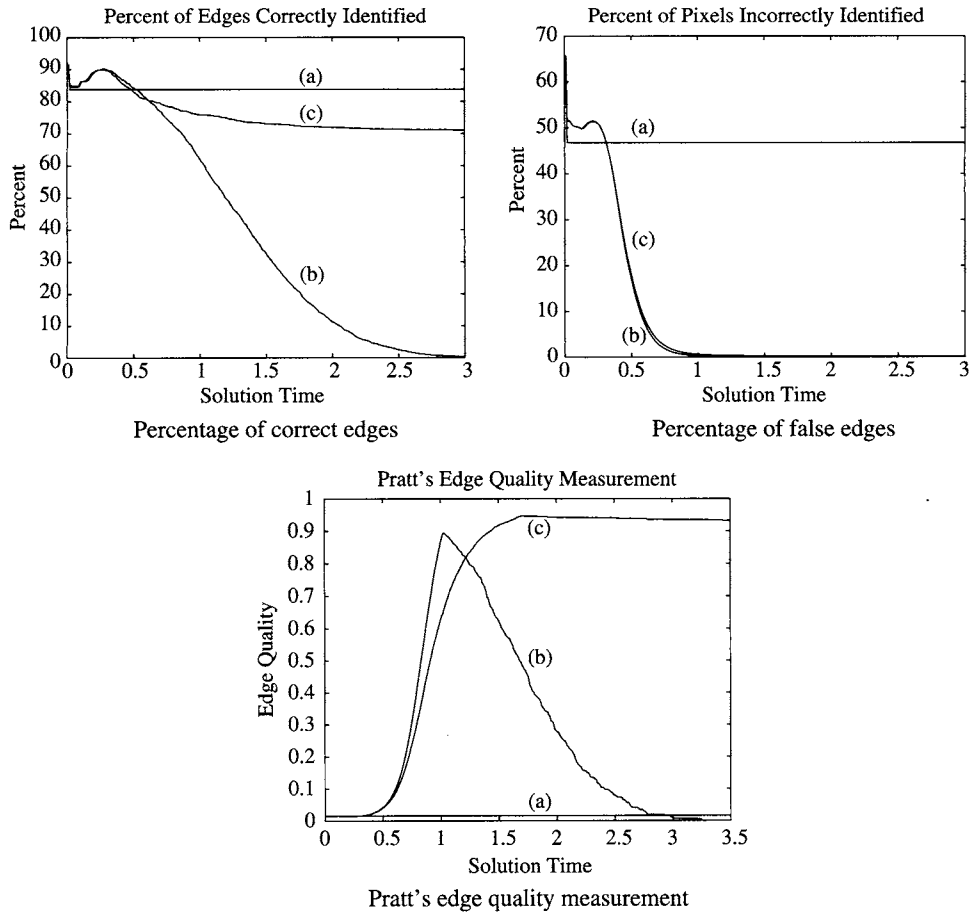


FIGURE 9 Edge detector performance vs. diffusion time for the results shown in Fig. 8. In the graphs, (a) corresponds to anisotropic diffusion with (9); (b) corresponds to (11) and (12); (c) corresponds to (11) and (13) [38].

experiment are presented in Fig. 9 for several solution times. It may be seen that the modified gradient coefficient [(11) and (12)] initially outperforms the other diffusion methods in the edge quality measurement, but produces the poorest identification percentage (due to the edge localization errors associated with the Gaussian filter). The morphologic anisotropic diffusion method [(11) and (13)] provides significant performance improvement, providing a 70% identification of true edges and a Pratt quality measurement of 0.95.

In summary, edges may be extracted from a diffused image by applying a heuristically selected threshold, by using a statistically motivated threshold, or by identifying features in the processed imagery. The success of the edge detection method can be evaluated qualitatively by visual inspection or quantitatively with edge quality metrics.

5 Using Vector Diffusion and Parametric Active Contours to Locate Edges

In this section, we discuss diffusion methods that drive a parametric active contour toward the boundary of a desired object. Instead of the diffusion of intensities or of gradient

magnitude, we utilize here the diffusion of vectors that point toward strong edges.

5.1 Parametric Active Contours

Active contours (or snakes) may be used to detect the edges forming an object boundary, given an initial guess (i.e., an initial contour). A parametric active contour is simply a set of contour points $[X(s), Y(s)]$ parameterized by $s \in [0,1]$. Typically, parametric active contours are implemented by finding the contour that minimizes $E = E_{\text{internal}} + E_{\text{external}}$, where E_{internal} is the internal energy of the active contour that quantifies the contour smoothness [21]:

$$E_{\text{internal}} = \frac{1}{2} \int_0^1 \left\{ \alpha \left[\left(\frac{dX(s)}{ds} \right)^2 + \left(\frac{dY(s)}{ds} \right)^2 \right] + \beta \left[\left(\frac{d^2X(s)}{ds^2} \right)^2 + \left(\frac{d^2Y(s)}{ds^2} \right)^2 \right] \right\} ds. \quad (41)$$

Here, α and β are two nonnegative weighting parameters expressing respectively the degree of the resistance to

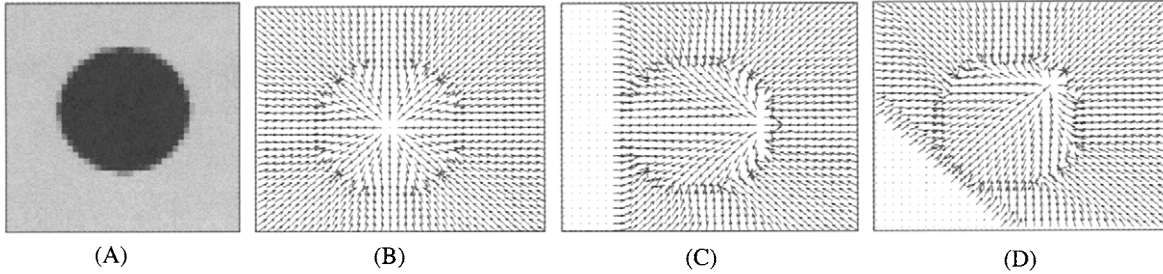


FIGURE 10 (A) A circle. (B) the external forces on the active contour after vector diffusion by GVF; (C) the external forces on the active contour after vector diffusion by MGVF with $(v^x, v^y) = (-1, -1)$.

stretching and bending of the contour. The external energy E_{External} is typically defined such that the contour seeks the edges in the image, I :

$$E_{\text{external}} = - \int_0^1 f(X(s), Y(s)) ds, \quad \text{where } f(x, y) = |\nabla I(x, y)|^2. \quad (42)$$

To minimize the contour energy ($= E_{\text{internal}} + E_{\text{external}}$), the calculus of variations [15][41] is applied to obtain the following Euler equations [21]:

$$-\alpha \frac{d^2 X}{ds^2} + \beta \frac{d^4 X}{ds^4} - \frac{\partial f}{\partial x} = 0, \quad -\alpha \frac{d^2 Y}{ds^2} + \beta \frac{d^4 Y}{ds^4} - \frac{\partial f}{\partial y} = 0. \quad (43)$$

To solve for the active contour positions such that (43) is satisfied, we can use PDEs for which $((X(s), Y(s))$ are treated as a function of time as well:

$$\frac{\partial X}{\partial t} = \alpha \frac{\partial^2 X}{\partial s^2} - \beta \frac{\partial^4 X}{\partial s^4} + u, \quad \frac{\partial Y}{\partial t} = \alpha \frac{\partial^2 Y}{\partial s^2} - \beta \frac{\partial^4 Y}{\partial s^4} + v. \quad (44)$$

Here, the external forces on the contour, $\partial f / \partial x$ and $\partial f / \partial y$, have been replaced by a force vector (u, v) . It is this vector that “points” to the desired edge. Fig. 10B shows the external forces generated by GVF for the circular target boundary shown in Fig. 10A.

5.2 Gradient Vector Flow

Diffusion can be used to capture an edge that is distant from the initial active contour. In this situation, the active contour is not driven toward the edge using (42), because the contour is not in “contact” with the gradient from the edge. To alleviate this problem, Xu and Prince construct a force field by diffusing the external force (u, v) , away from edges into the homogeneous regions, while at the same time retaining the initial external force at the boundaries. This vector diffusion

is achieved by minimizing [45]

$$E_{\text{GVF}}(u, v) = \frac{1}{2} \iint \mu(u_x^2 + u_y^2 + v_x^2 + v_y^2) + (f_x^2 + f_y^2)((u - f_x)^2 + (v - f_y)^2) dx dy, \quad (45)$$

where μ is a nonnegative parameter expressing the degree of smoothness of the field (u, v) (and can be replaced by an edge-sensitive diffusion coefficient [46]), and f is the edge-map as defined in (42). The interpretation of (45) is straightforward — the first term keeps the vector field, (u, v) , smooth, while the second term forces it to be close to the external forces near the edges (i.e., where the edge-force strength is high). Variational minimization of (2.19) results in the following two Euler equations [45]:

$$\mu \nabla^2 u - (f_x^2 + f_y^2)(u - f_x) = 0, \quad \mu \nabla^2 v - (f_x^2 + f_y^2)(v - f_y) = 0. \quad (46)$$

Solving (46) for (u, v) results in vector diffusion process called gradient vector flow (GVF). The resulting (u, v) vectors can be used as the external force in (44). Figs. 10C and 10D show the external forces for a circular object for two directions of motion.

5.3 Motion Gradient Vector Flow

GVF can be modified to track a moving object boundary in a video sequence. Here, we assume that the direction of object motion (v^x, v^y) is known. Instead of computing the components of external force (u and v) separately, we utilize a vector ∇w , which is the gradient of a computed quantity w (at each point in the image). To obtain w , we minimize

$$E_{\text{MGVF}}(w) = \frac{1}{2} \iint [\mu H_\epsilon(\nabla w \cdot (v^x, v^y)) |\nabla w|^2 + f(w - f)^2] dx dy \quad (47)$$

where H_ϵ is a regularized Heaviside (step) function, f is the squared image gradient magnitude as defined in (42), and μ is

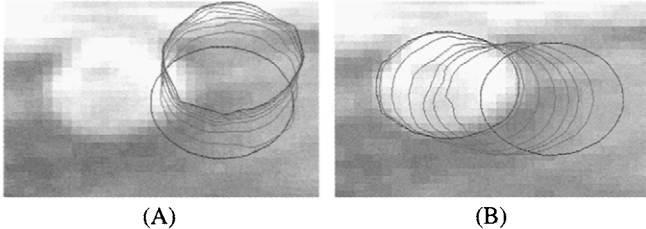


FIGURE 11 (A) In tracking a white blood cell, the GVF vector diffusion fails to attract the active contour; (B) Successful detection is yielded by MGVF.

a weight on smoothness of the vector field. The first term in (47) encourages diffusion of motion gradient vectors in the direction of flow, and discourages diffusion in the opposite direction. The second term forces the magnitude of w to resemble that of f , the edge strength, where f is high in magnitude.

A gradient descent update for w is derived by way of variational calculus:

$$\frac{\partial w}{\partial t} = \mu \operatorname{div}(H_\varepsilon(\nabla w \cdot (v^x, v^y)) \nabla w) - f(w - f). \quad (48)$$

So, (48) provides an external force that can guide an active contour to a moving object boundary. The capture range of gradient vector flow is increased using the motion gradient vector flow (MGVF) vector diffusion [33]. With MGVF, a tracking algorithm can simply use the final position of the active contour from a previous video frame as the initial contour in the subsequent frame. For an example of tracking using MGVF, see Fig. 11.

6 Conclusions

Anisotropic diffusion is an effective precursor to edge detection. The main benefit of anisotropic diffusion over isotropic diffusion and linear filtering is edge preservation. By properly specifying the diffusion PDE and the diffusion coefficient, an image can be scaled, denoised, and simplified for boundary detection. For edge detection, the most critical design step is specification of the diffusion coefficient. The variants of the diffusion coefficient involve tradeoffs between sensitivity to noise, the ability to specify scale, convergence issues, and computational cost. The diverse implementations of the anisotropic diffusion PDE result in improved fidelity to the original image, mean curvature motion, and convergence to locally monotonic signals. As the diffusion PDE may be considered a descent on an energy surface, the diffusion operation can be viewed in a variational framework. Recent variational solutions produce optimized edge maps and image segmentations in which certain edge-based features, such as edge length, curvature, thickness, and connectivity, can be optimized.

The computational cost of anisotropic diffusion may be reduced by using multiresolution solutions, including the anisotropic diffusion pyramid and multigrid anisotropic diffusion. Application of edge detection to multispectral imagery and to radar/ultrasound imagery is possible through techniques presented in the literature. In general, the edge detection step after anisotropic diffusion of the image is straightforward. Edges may be detected using a simple gradient magnitude threshold, using robust statistics, or using a feature extraction technique. Active contours, used in conjunction with vector diffusion, can be used to extract meaningful object boundaries.

References

- [1] S. T. Acton, "Locally monotonic diffusion," *IEEE Trans. Signal Process.* 48, 1379–1389 (2000).
- [2] S. T. Acton, "Multigrid anisotropic diffusion," *IEEE Trans. Image Process.* 7, 280–291 (1998).
- [3] S. T. Acton, "A pyramidal edge detector based on anisotropic diffusion," *Proceedings of the IEEE International Conference on Acoustics, Speech and Signal Processing (ICASSP-96)* (Atlanta, May 7–10, 1996).
- [4] S. T. Acton, A. C. Bovik, and M. M. Crawford, "Anisotropic diffusion pyramids for image segmentation," *Proceedings of the IEEE International Conference on Image Process* (Austin, Texas, Nov. 1994).
- [5] S. T. Acton and A. C. Bovik, "Anisotropic edge detection using mean field annealing," *Proc. of the IEEE International Conference on Acoustics, Speech and Signal Process (ICASSP-92)* (San Francisco, March 23–26, 1992).
- [6] S. T. Acton and J. Landis, "Multispectral anisotropic diffusion," *Int. J. Remote Sensing* 18, 2877–2886 (1997).
- [7] L. Alvarez, P.-L. Lions, and J.-M. Morel, "Image selective smoothing and edge detection by nonlinear diffusion II," *SIAM J. Numer. Anal.* 29, 845–866 (1992).
- [8] M. J. Black, G. Sapiro, D. H. Marimont, and D. Heeger, "Robust anisotropic diffusion" *IEEE Trans. Image Process.* 7, 421–432 (1998).
- [9] J. H. Bramble, *Multigrid Methods* (John Wiley, New York, 1993).
- [10] P. J. Burt, T. Hong, and A. Rosenfeld, "Segmentation and estimation of region properties through cooperative hierarchical computation," in *IEEE Trans. Systems Man. Cybern.* 11, 802–809, (1981).
- [11] P. J. Burt, "Smart Sensing within a Pyramid Vision Machine," in *Proceedings of the IEEE*, 76, 1006–1015 (1988).
- [12] J. Canny, "A computational approach to edge detection," *IEEE Trans. Pattern Anal. Mach. Intell. PAMI-8*, 679–691, (1986).
- [13] V. Caselles, J.-M. Morel, G. Sapiro, and A. Tannenbaum, "Introduction to the special issue on partial differential equations and geometry-driven diffusion in image processing and analysis," *IEEE Trans. Image Process.* 7, 269–273 (1998).
- [14] F. Catte, P.-L. Lions, J.-M. Morel, and T. Coll, "Image selective smoothing and edge detection by nonlinear diffusion, *SIAM J. Numer. Anal.* vol. 29, 182–193 (1992).
- [15] R. Courant and D. Hilbert, *Methods of Mathematical Physics* (Interscience Publishers, New York, 1953).

- [16] S. DiZzenzo, "A note on the gradient of a multiimage," *Comput. Vis. Graph. Image Process.* 33, 116–125 (1986).
- [17] A. El-Fallah and G. Ford, "The evolution of mean curvature in image filtering," *Proceedings of the IEEE International Conference on Image Process* (Austin, Texas, Nov. 1994).
- [18] D. Geman and G. Reynolds, "Constrained restoration and the recovery of discontinuities," *IEEE Trans. Pattern Anal. Mach. Intell.* 14, 376–383 (1992).
- [19] W. Hackbusch and U. Trottenberg, eds., *Multigrid Methods* (Springer-Verlag, New York, 1982).
- [20] R. M. Haralick, X. Zhuang, C. Lin, and J. S. J. Lee, "The digital morphological sampling theorem," *IEEE Trans. Acoust. Speech Signal Process.* 37, 2067–2090 (1989).
- [21] M. Kass, A. Witkin, and D. Terzopoulos, "Snakes: Active contour models," *Int. J. Comput. Vis.* 321–331 (1987).
- [22] J. J. Koenderink, "The structure of images," *Biol. Cybern.* 50, 363–370 (1984).
- [23] D. G. Lowe, *Perceptual Organization and Visual Recognition* (Kluwer Academic, New York, 1985).
- [24] D. Marr and E. Hildreth, "Theory of edge detection," *Proc. Royal Soc. London.* B207, 187–217 (1980).
- [25] A. Morales, R. Acharya, and S. Ko, "Morphological pyramids with alternating sequential filters," in *IEEE Trans. Image Process.* 4, 965–977 (1996).
- [26] J.-L. Morel and S. Solimini, *Variational Methods in Image Segmentation* (Birkhauser, Boston, 1995).
- [27] D. Mumford and J. Shah, "Boundary detection by minimizing functionals," *IEEE Int. Conference on Computer Vision and Pattern Recognition* (San Francisco, 1985).
- [28] K. N. Nordstrom, "Biased anisotropic diffusion — a unified approach to edge detection," *Dept. of Electrical Engineering and Computer Sciences Tech. Report* (University of California at Berkeley, Berkeley, CA, 1989).
- [29] S. Osher and L.-I. Rudin, "Feature-oriented image enhancement using shock filters," *SIAM J. Numeric. Anal.* 27, 919–940 (1990).
- [30] S. Osher and J. Sethian, "Fronts propagating with curvature dependent speed: algorithms based on the Hamilton-Jacobi formulation," *J. Comp. Physics* 79, 12–49 (1988).
- [31] P. Perona and J. Malik, "Scale-space and edge detection using anisotropic diffusion," *IEEE Trans. Pattern Anal. Mach. Intell. PAMI-12*, 629–639 (1990).
- [32] W. K. Pratt, *Digital Image Process* (Wiley, New York, 1978), 495–501.
- [33] N. Ray and S. T. Acton, "Motion gradient vector flow: an external force for tracking rolling leukocytes with shape and size constrained active contours," *IEEE Transactions on Medical Imaging*, 23, 1466–1478 (2004).
- [34] P. J. Rousseeuw and A. M. Leroy, *Robust Regression and Outlier Detection* (Wiley, New York, 1987).
- [35] L.-I. Rudin, S. Osher, and E. Fatemi, "Nonlinear total variation noise removal algorithm," *Physica D* 60, 1217–1229 (1992).
- [36] G. Sapiro and D. L. Ringach, "Anisotropic diffusion of multi-valued images with applications to color filtering," *IEEE Trans. Image Process.* 5, 1582–1586 (1996).
- [37] C. A. Segall, S. T. Acton, and A. K. Katsaggelos, "Sampling conditions for anisotropic diffusion," *Proceedings of the SPIE Symposium on Visual Communications and Image Process* (San Jose, CA, January 23–29, 1999).
- [38] C. A. Segall and S. T. Acton, "Morphological anisotropic diffusion," *Proceedings of the IEEE International Conference on Image Processing* (Santa Barbara, CA, October 26–29, 1997).
- [39] N. Sochen, R. Kimmel, and R. Malladi, "A general framework for low level vision," *IEEE Trans. Image Process.* 7, 310–318 (1998).
- [40] S. Teboul, L. Blanc-Feraud, G. Aubert, and M. Barlaud, "Variational approach for edge-preserving regularization using coupled PDE's," *IEEE Trans. Image Process.* 7, 387–397 (1998).
- [41] J. L. Troutman, *Variational Calculus with Elementary Convexity* (Springer-Verlag, New York, 1983).
- [42] R. T. Whitaker and S. M. Pizer, "A multiscale approach to nonuniform diffusion," *Comput. Vis. Graph. Image Process.* 57, 99–110 (1993).
- [43] R. T. Whitaker and G. Gerig, "Vector-valued diffusion," in *Geometry-Driven Diffusion in Computer Vision*, Bart ter Haar Romeny, ed., (Kluwer, New York, 1994), 93–134.
- [44] A. P. Witkin, "Scale-space filtering," in *Proc. Int. Joint Conf. Artif. Intell.* 1019–1021 (1983).
- [45] C. Xu and J. L. Prince, "Snakes, shapes, and gradient vector flow," *IEEE Trans. Image Process.* 7, 359–369 (1998).
- [46] C. Xu and J. L. Prince, "Generalized gradient vector flow external force for active contours," *Signal Process.* 71, 131–139 (1998).
- [47] A. Yezzi, Jr., "Modified curvature motion for image smoothing and enhancement," *IEEE Trans. Image Process.* 7, 345–352 (1998).
- [48] Y.-L. You, W. Xu, A. Tannenbaum, and M. Kaveh, "Behavioral analysis of anisotropic diffusion in image processing," *IEEE Trans. Image Process.* 5, 1539–1553 (1996).
- [49] Y.-L. You, M. Kaveh, W. Xu, and A. Tannenbaum, "Analysis and design of anisotropic diffusion for image processing," *Proceedings of the IEEE International Conference on Image Processing* (Austin, Texas, November 13–16, 1994).
- [50] Y. Yu and S. T. Acton, "Speckle reducing anisotropic diffusion," *IEEE Trans. Image Process.* 11, 1260–1270 (2002).
- [51] Y. Yu and S. T. Acton, "Edge detection in ultrasound imagery using the instantaneous coefficient of variation," *IEEE Trans. Image Process.* 13, 1640–1655 (2004).

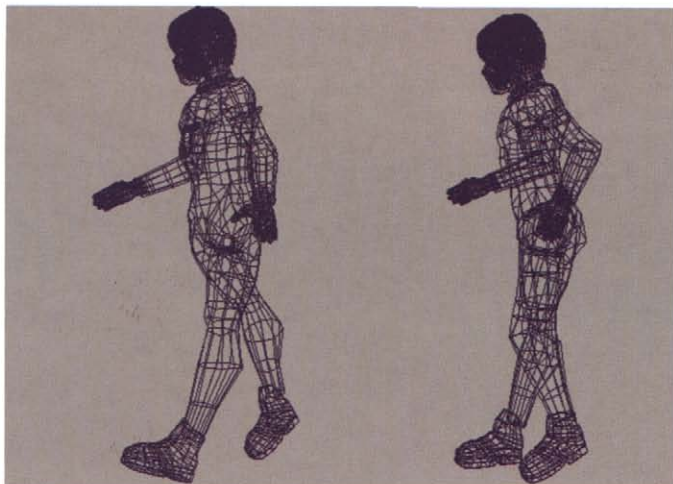


FIGURE 4.11.9 Polygonal representation of the human body, adapted from [124].

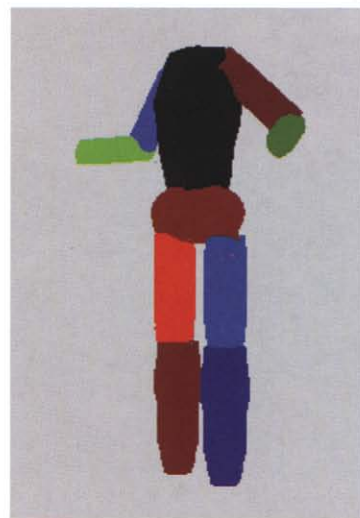


FIGURE 4.11.10 Cylinder-based volumetric representation of the human body.

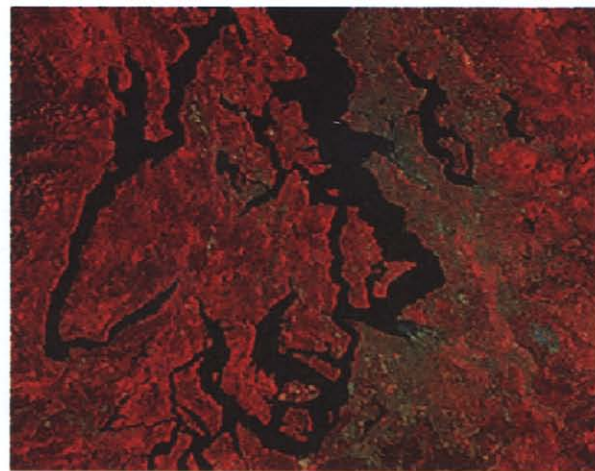
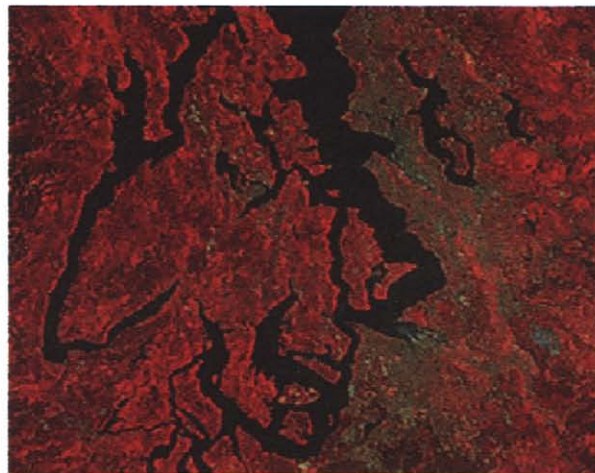


FIGURE 4.14.4 (top) SPOT multispectral image of the Seattle area, with additive Gaussian-distributed noise, $\sigma = 10$.
(bottom) Vector distance dissimilarity diffusion result, using diffusion coefficient in (9).